No. 685 **February 2026**

Generating fully developed flow profiles for simulations of viscoelastic fluids described by differential models

P. Westervoß, H. Damanik,
O. Mierka, A. Ouazzi, S. Turek

ISSN: 2190-1767

Generating fully developed flow profiles for simulations of viscoelastic fluids described by differential models

P. Westervoß, H. Damanik, O. Mierka, A. Ouazzi, S. Turek

Institute of Applied Mathematics (LS III), TU Dortmund University, Vogelpothsweg 87, D-44227 Dortmund, Germany

Abstract

In this paper, an iterative method is developed to compute the flow profiles of a viscoelastic fluid without solvent part described by various differential models in case of a two-dimensional fully developed channel flow. Therefore, the tensorial formulation of the models for the conformation tensor is written as a nonlinear one dimensional system of equations for the unknown components of the conformation tensor, the pressure and the velocity field. On the basis of an initial guess for the pressure drop, the unknown quantities can be determined iteratively. For sufficiently high relaxation times, the resulting flow profiles show typical viscoelastic behaviour. Furthermore, corresponding two-dimensional Finite Element simulations of a Poiseuille flow through a plane channel are used to perform a validation of the determined flow profiles for the Giesekus model.

Keywords: flow profiles, viscoelastic fluid, Giesekus model, shear thinning, polymer melt

1. Introduction and motivation

The choice of boundary conditions plays an important role in the context of simulating the behaviour of fluids (c.f. [7]). If incorrect boundary conditions are applied, this could lead to inappropriate results in numerical simulations, which therefore do not represent actual physical effects. For example, in case of the simulation of a Poiseuille flow of a viscoelastic fluid described by the Giesekus model, the application of a parabolic in- and outflow profile for the velocity induces the numerical results depicted in figure 1. It becomes clear, that the chosen parabolic velocity profile is not suitable for the applied Giesekus model, because away from the in- and outflow edge the velocity field takes a differing shape. This is contradictory to the expected numerical results, which should show the prescribed parabolic profile in the whole domain, i.e. the contour lines should be

Email addresses: patrick.westervoss@math.tu-dortmund.de (P. Westervoß), hogenrich.damanik@math.tu-dortmund.de (H. Damanik), otto.mierka@math.tu-dortmund.de (O. Mierka), abderrahim.ouazzi@math.tu-dortmund.de (A. Ouazzi), stefan.turek@math.tu-dortmund.de (S. Turek)

straight lines. But obviously, especially in the middle of the domain, the obtained profile deviates from the parabolic form and shows backflow and even numerical oscillations. Furthermore, the same behaviour can be observed for the stress field, which is why for these variables suitable flow profiles need to be determined as well, which can be used as in- and outflow profiles for the stress variable.

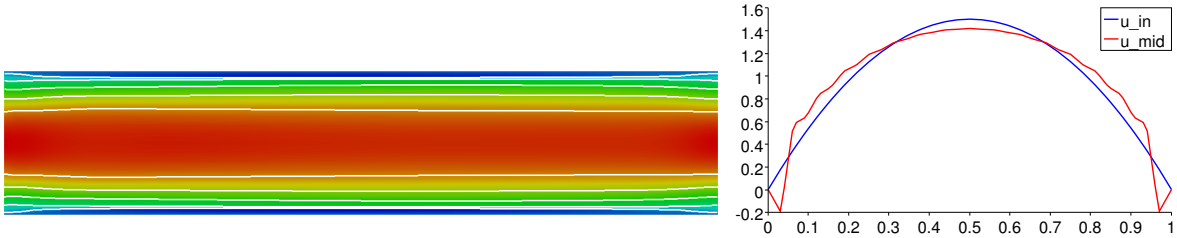

(a) contour lines

(b) profiles at $x = 0$ and $x = 2.5$

Figure 1: velocity field for Giesekus model with parabolic inflow, $\Lambda = 0.5$, $\alpha = 0.1$

Hence, in this report a method is presented to determine fully developed flow profiles for viscoelastic fluids, which can then be applied as suitable in- and outflow profiles for various viscoelastic models in numerical simulations. In the first place, we restrict ourselves to viscoelastic fluids which are pure polymer melts, i.e. these fluids do not contain any solvent material, and are modeled with the Giesekus model (c.f. [8]). But in contrast to other works, we will transfer the method to allow the determination of flow profiles for other differential models like FENE (c.f. [9]) or PTT (c.f. [10]) and will also consider viscoelastic fluids which contain solvent part. Both extensions of the primary method represent new features in determining fully developed flow profiles for viscoelastic fluids.

To model the behaviour of such fluids, we utilize the Stokes equations coupled with an additional equation, which specifies the used material model (c.f. [3]). As far as the use of the Oldroyd-B model for Poiseuille flow is concerned, the resulting fully developed flow profiles are given analytically: the velocity profile is given in a parabolic manner and the stresses can be derived in an analytical way (c.f. [1],[3]). Due to that, the fully developed profiles can be applied as correct boundary conditions. But as soon as actual nonlinear models are concerned, these variables can in general not be expressed by analytical functions (c.f. [2], [5]). Because of shear effects, the velocity profile differs from the parabolic form, which arises in case of the Oldroyd-B model. Also the stresses can not be described analytically, because the mentioned models obey a nonlinear dependence on the stress tensor which needs to be solved.

In this paper, we want to present a method to calculate numerically the velocity and stress profiles which appear in a fully developed flow of a viscoelastic fluid described by nonlinear differential models. These profiles can be used as boundary conditions in

numerical simulations to guarantee a fully developed inflow (and outflow) profile.

As numerical test case we consider the flow through a rectangular channel in the (x, y) plane of height 1 and infinite length. Because of the symmetry of the domain we only consider half of the channel, i.e. a cross section of the channel can be described by a certain position $x \in \mathbb{R}$ together with a variable $y \in [0, 0.5]$. Thus, all flow profiles at such cutlines are definied on $[0, 0.5]$ as well.

The structure of the paper is as follows. In section 2 we will derive the basic numerical method to determine fully developed flow profiles of viscoelastic fluids on the basis of the Giesekus model for pure polymer melts. Therefore, the governing equations are pointed out and are formulated as a nonlinear system of ordinary differential equations, which will be solved numerically. Afterwards, the derived method will be transferred to further differential models. In the next section 3, a solvent, i.e. Newtonian, part is introduced into the considered fluids and the adapted numerical method to determine the corresponding flow profiles as well as numerical results are presented. As a final step, the flow profiles obtained for the Giesekus model are validated by actual two-dimensional Finite Element simulations in section 4. In section 5, we will summarize the main results of this work and give an outlook on further applications and improvements of the presented method.

2. Derivation of the method and discussion of results

The derivation of the numerical method presented in the following will be executed on the example of the Giesekus model. In section 2.1, the corresponding equations are introduced and transformed into a nonlinear ODE system, which will be solved numerically in section 2.2. This solution process results in a method to calculate fully developed flow profiles of a viscoelastic fluid flow described by the Giesekus model. Flow profiles obtained in this manner are analyzed in section 2.3. Afterwards, in section 2.4, the previously derived method is applied to the FENE and PTT model.

2.1. Governing equations

The starting point of the following remarks are the stationary Stokes equations

$$\frac{1}{\rho}\nabla p = \frac{1}{\rho}\nabla \cdot \mathbf{T}, \qquad \nabla \cdot \mathbf{u} = 0, \tag{1}$$

which relate the pressure p, the velocity field $\mathbf{u}$, the extra stress tensor $\mathbf{T}$ and the density ρ of the fluid with each other (c.f. [6]). In the following, we set $\rho = 1$. According to [3], the extra stress tensor for pure melts, i.e. such fluids, that do not contain any solvent material, can be written in the form

$$\mathbf{T} = \frac{\eta_p}{\Lambda}(\boldsymbol{\tau} - \mathbf{I}) \tag{2}$$

with the polymer viscosity η_p, the relaxation time Λ and the conformation tensor $\boldsymbol{\tau}$ of the fluid. If we insert equation (2) into equation (1) we get

$$\begin{aligned} \nabla p &= \frac{\eta_p}{\Lambda} \nabla \cdot \boldsymbol{\tau}, && \text{(3a)} \\ \nabla \cdot \mathbf{u} &= 0. && \text{(3b)} \end{aligned}$$

The choice of the material model is specified by an additional equation for the conformation tensor $\boldsymbol{\tau}$. We intend to use the Giesekus model for fully developed stationary flows, which is why the equation for the conformation tensor reads

$$-\nabla \mathbf{u} \cdot \boldsymbol{\tau} - \boldsymbol{\tau} \cdot \nabla \mathbf{u}^\top + \frac{1}{\Lambda} \left(\boldsymbol{\tau} - \mathbf{I} + \alpha \left(\boldsymbol{\tau} - \mathbf{I} \right)^2 \right) = \mathbf{0} \tag{4}$$

with $\alpha \in [0, 1]$ (c.f. [3]).

As a next step we use the equations (3a) and (4) to derive a method for computing fully developed flow profiles for pure polymer melts.

2.2. The numerical method

Because we consider a fully developed two-dimensional flow, the occuring vector fields are independent of the x-variable and thus we assume

$$\mathbf{u} = \begin{pmatrix} u \\ v \end{pmatrix} = \begin{pmatrix} u\left(y\right) \\ 0 \end{pmatrix}, \quad \frac{\partial u}{\partial x} = \frac{\partial v}{\partial x} = \frac{\partial v}{\partial y} = 0, \quad \frac{\partial \tau_{ij}}{\partial x} = 0 \text{ for } i, j \in \{1, 2\} \tag{5}$$

Furthermore, we assume that the pressure in an infinite channel is linear in x, so that

$$p\left(x, y\right) = a + bx + f_p\left(y\right) \tag{6}$$

holds with $a, b \in \mathbb{R}$ and a suitable function $f_p : \mathbb{R} \to \mathbb{R}$, which implies $\frac{\partial p}{\partial x} = \text{const}$. When we write equation (3a) component-by-component with respect to equation (5), we get

$$\begin{aligned} \frac{\partial p}{\partial x} &= \frac{\eta_p}{\Lambda} \frac{\partial \tau_{12}}{\partial y}, && \text{(7a)} \\ \frac{\partial p}{\partial y} &= \frac{\eta_p}{\Lambda} \frac{\partial \tau_{22}}{\partial y}, && \text{(7b)} \end{aligned}$$

which is why τ_{12} is linear in y due to $\frac{\partial p}{\partial x} = \text{const}$ and this component of the conformation tensor $\boldsymbol{\tau}$ can be computed explicitly for given $\frac{\partial p}{\partial x}$. This is done by integrating $\frac{\partial \tau_{12}}{\partial y}$ with

respect to y under the condition $\tau_{12}(0.5) = 0$, which is based on the fact that the shear stress vanishes on the centerline of the channel. Furthermore, we can conclude from equation (7b), that the function f_p, which defines the y-dependency of the pressure in equation (6), is a function of τ_{22}. In the following we assume $f_p(0.5) = 0$, which leads to

$$p(x,y) = a + bx + \frac{\eta_p}{\Lambda}\left(\tau_{22}(y) - 1\right). \tag{8}$$

In the derivation of equation (8) we used the fact, that the conformation tensor $\boldsymbol{\tau}$ is positive definit by construction (c.f. [4]) to guarantee, that $\tau_{22}(0.5) = 1.0$ for $\alpha \in [0,1]$. This can be concluded from equation (9c), because otherwise the positive-definiteness of the conformation tensor would be violated.

As a next step, we rewrite equation (4) of the Giesekus model component-by-component with respect to equation (5), which results in the three equations

$$\begin{aligned}
-2\tau_{12}\frac{\partial u}{\partial y} + \frac{1}{\Lambda}\left[\tau_{11} - 1 + \alpha\left(\left(\tau_{11}-1\right)^2 + \tau_{12}^2\right)\right] &= 0 && \text{(9a)}\\
-\tau_{22}\frac{\partial u}{\partial y} + \frac{1}{\Lambda}\left[\tau_{12} + \alpha\left(\left(\tau_{11}-1\right)\tau_{12} + \tau_{12}\left(\tau_{22}-1\right)\right)\right] &= 0 && \text{(9b)}\\
\frac{1}{\Lambda}\left[\tau_{22} - 1 + \alpha\left(\tau_{12}^2 + \left(\tau_{22}-1\right)^2\right)\right] &= 0. && \text{(9c)}
\end{aligned}$$

From the equations (9), we can determine the remaining unknowns τ_{22}, τ_{11} and $\frac{\partial u}{\partial y}$ in the following way: First we compute τ_{22} from equation (9c) with the help of the previously determined τ_{12}. Then we solve the equations (9a) and (9b) for $\frac{\partial u}{\partial y}$ and equalize the resulting equations to calculate τ_{11}. At last we use equation (9a) or (9b) to determine the last unknown $\frac{\partial u}{\partial y}$. Finally we get the complete velocity profile $u(y)$ by integrating $\frac{\partial u}{\partial y}$ in consideration of the boundary condition $u(0) = 0$. This condition holds, because we force the velocity to vanish on the wall of the channel.

Unfortunately, the pressure drop $\frac{\partial p}{\partial x}$ is a priori unknown for many configurations. That is why we can not use the actual pressure drop to compute the velocity profile u. But we can apply an iterative method to determine the correct pressure drop $\frac{\partial p}{\partial x}$ and thereby the desired velocity profile.

Hence, we make an initial guess for $\frac{\partial p}{\partial x}$ and compute the resulting velocity profile with equations (7a) and (9). Now we need to derive a condition to check if the velocity profile matches the considered test case. This can be done by normalizing the Reynolds number of the flow and thus defining a fixed value for the flow rate, e.g.

$$\dot{U} = \int_0^{0.5} u(y)\,\mathrm{d}y = 0.5. \tag{10}$$

We can check this condition by integrating the calculated velocity field. If the condition (10) is not fulfilled, we correct the initial guess of $\frac{\partial p}{\partial x}$ in a suitable manner. We repeat this procedure, until the calculated velocity field fulfills the criterion (10). This approach leads to an iterative method to compute the fully developed velocity field if the Giesekus model is used.

The last open question is how to derive a correction technique for $\frac{\partial p}{\partial x}$ if the calculated flow rate differs from the prescribed one. This is realized by calculating the derivative of the flow rate with respect to the pressure drop. Then we use this derivative to extrapolate the calculated flow rate to the desired value. If the initial value for $\frac{\partial p}{\partial x}$ was not close enough to the real value, we would perform a large correction step. We can avoid this by inserting a relaxation parameter $\omega \in]0, 1]$.

The complete described method is given in algorithm 1.

Algorithm 1 computing flow profiles for the Giesekus model

set $i = 0$ and choose $\left(\frac{\partial p}{\partial x}\right)_i$, a tolerance TOL, $\varepsilon > 0$ and $\omega \in]0, 1]$
set desired flow rate $\dot{U} = 0.5$, set initial approximate flow rate $\bar{U} = 1.0$
while $|\dot{U} - \bar{U}| > TOL$ **do**
    for $j = 1, 2$ **do**
        set $\left(\frac{\partial p}{\partial x}\right)_i = \left(\frac{\partial p}{\partial x}\right)_i + (j-1)\,\varepsilon$
        determine $(\tau_{12})_i$ from equation (7a) with respect to $\tau_{12}(0.5) = 0$
        compute $(\tau_{22})_i$ from equation (9c) as well as $(\tau_{11})_i$ and $\left(\frac{\partial u}{\partial y}\right)_i$ from equation (9b) and (9a)
        calculate u_i by integrating $\left(\frac{\partial u}{\partial y}\right)_i$ with $u(0) = 0$
        determine $\bar{U}_j = \int_0^{0.5} u_i(y)\,\mathrm{d}y$
    end for
    set $\bar{U} = \bar{U}_1$ and calculate $\partial\bar{U} := \frac{\bar{U}_2 - \bar{U}_1}{\varepsilon}$
    set $\left(\frac{\partial p}{\partial x}\right)_{i+1} = \left(\frac{\partial p}{\partial x}\right)_i + \omega\frac{\dot{U} - \bar{U}}{\partial\bar{U}}$
    set $i = i + 1$
end while

2.3. Computational results

In this section, we want to give some results of the method explained beforehand, to show that profiles can be obtained, which deviate from the parabolic one and have a behaviour typical for the Giesekus model. Therefore, velocity profiles obtained with algorithm 1 are compared with the parabolic profile

$$u(y) = 6y(1-y), \quad y \in [0, 0.5] \tag{11}$$

of the Oldroyd-B model, which results in a flux of $\dot{U} = 0.5$. For completeness, the corresponding stress and pressure profiles, i.e. the course of the function f_p, for the Giesekus model are given as well.

Some examples of flow profiles resulting from the method described in section 2.2 are given in figure 2, where fully developed flow profiles for various values of Λ are presented, while the additional parameters $\alpha = 0.01$ and $\eta_p = 1.0$ are kept fixed.

For increasing Λ, a typical shear thinning behaviour can be observed, which is one of the main properties predicted by the Giesekus model. In case of shear thinning, the velocity profile deviates from the parabolic profile, such that the velocity increases steeper near the wall of the channel, but shows a flatter behaviour in the middle.

Beside the shear thinning effect, we can observe, that the stress values increase for increasing Λ, which also occurs for the Oldroyd-B model. This can directly be concluded from the analytical expressions for the stress components for the Oldroyd-B model, which are derived in [3]. Another difference between the Giesekus and the Oldroyd-B model can be observed with respect to the pressure. On the basis of the function f_p, which is also pictured in figure 2 and occurs in the pressure function (6) or (8), respectively, it becomes clear, that the pressure depends not only on x, but shows an actual y-dependency as well. This is in contrast to the Oldroyd-B model, where the pressure is constant with respect to y.

Up to now we can state, that the determined flow profiles show physically reasonable properties, which in some cases correlate to the behaviour for the Oldroyd-B model. But at the same time we clearly see differences between the profiles resulting from the different models.

Previously, we analyzed the effect of the relaxation time Λ on the flow profiles. Next, we want to investigate the influence of the Giesekus parameter α. Therefore, we fix again the polymer viscosity to $\eta_p = 1.0$ and, additionally, set the relaxation time to $\Lambda = 0.1$.

First, we consider the case $\alpha = 0.0$. It can be easily seen from equation (4), that the Giesekus model for pure melts and $\alpha = 0.0$ coincides with the Oldroyd-B or Upper Convected Maxwell model, respectively (c.f. [8]). Hence, for $\alpha = 0.0$, the flow profiles obtained with algorithm 1 should match the profiles resulting from the Oldroyd-B model, i.e. the velocity profile should take the parabolic form in equation (11) and the pressure should be constant with respect to y. Furthermore, τ_{11} should have a quadratic, τ_{12} a linear behaviour and τ_{22} should be constant. As can be seen in figure 3(a), this behaviour of the numerically determined profiles can be observed.

Compared to figure 2(b) and 2(c), the increase of α has a similar effect on the velocity profile as increasing Λ. Additionally, the slope of the velocity and stresses near the wall of the channel increases for increasing α, which also holds for increasing Λ. In contrast, the stress values decrease for increasing α and the order of the pressure values increases.

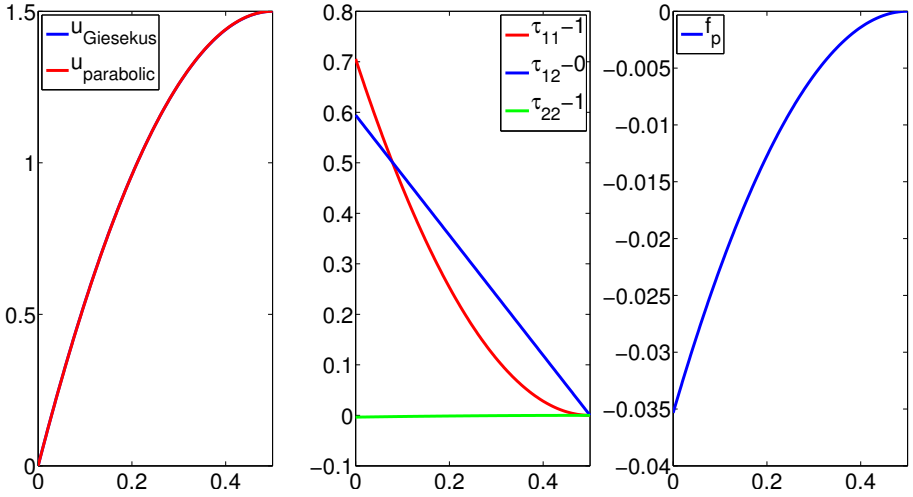

(a) $\Lambda = 0.1$

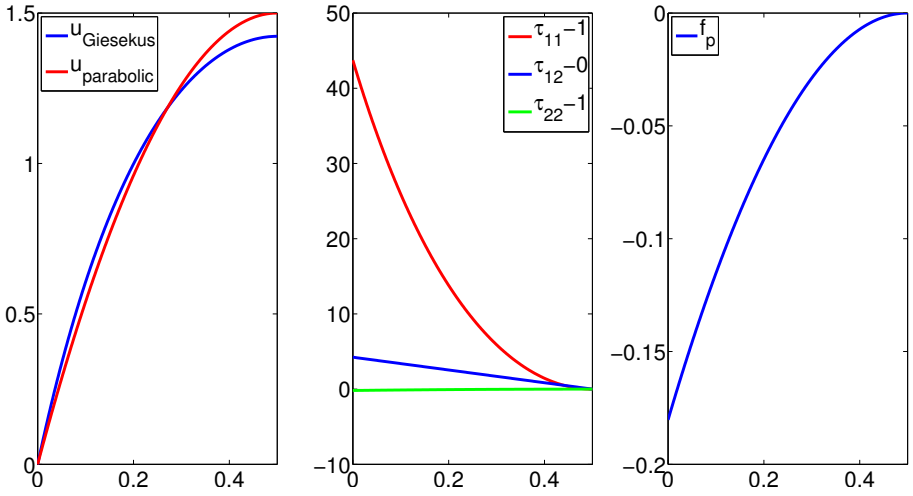

(b) $\Lambda = 1.0$

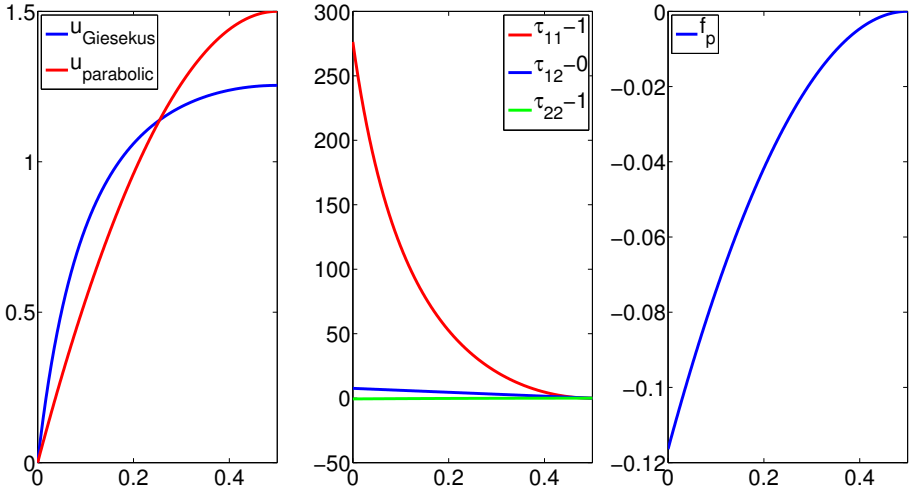

(c) $\Lambda = 5.0$

Figure 2: flow profiles for various Λ, $\alpha = 0.01$ and $\eta_p = 1.0$

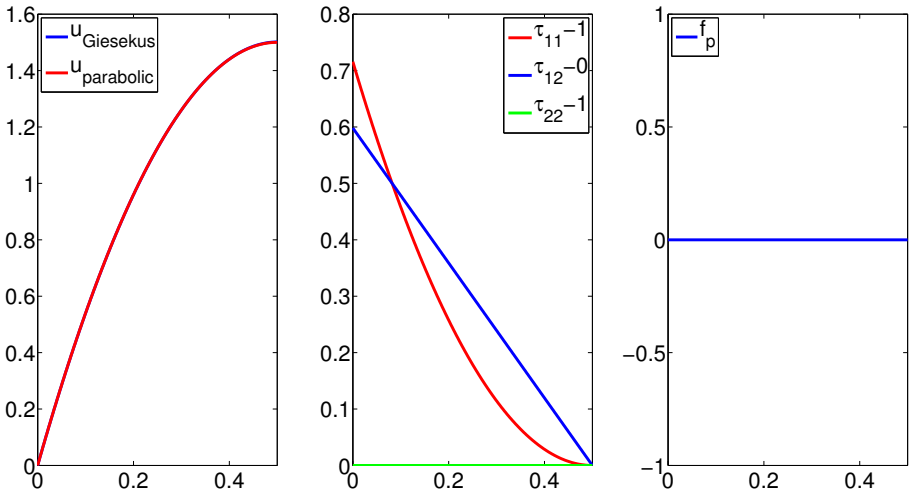

(a) $\alpha = 0.0$

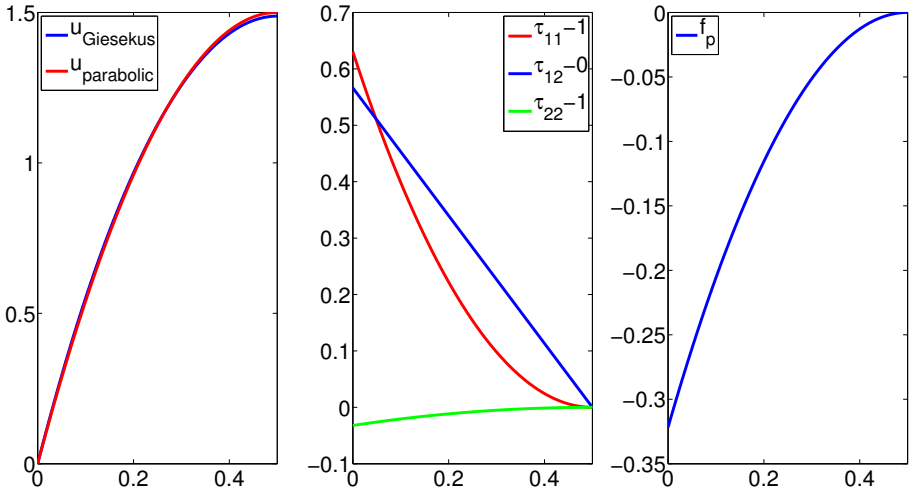

(b) $\alpha = 0.1$

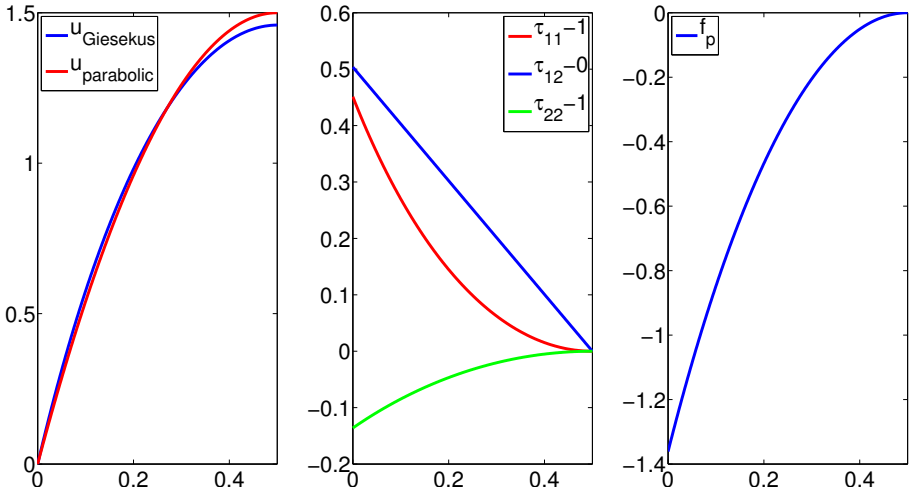

(c) $\alpha = 0.5$

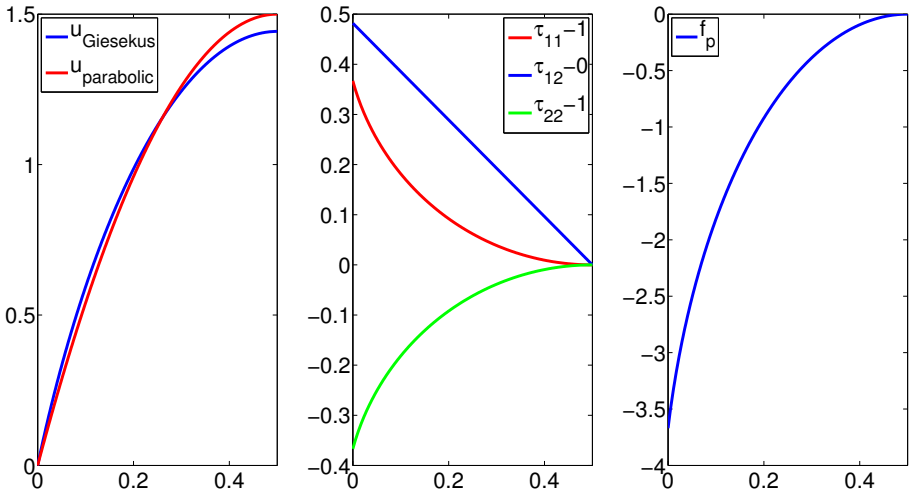

(d) $\alpha = 1.0$

Figure 3: flow profiles for $\Lambda = 0.1$, various α and $\eta_p = 1.0$

In figures 4(a) and 4(b), an overview of the different velocity profiles generated for various combinations of values of Λ and α is given. If both parameters are chosen small, the profile matches the parabolic shape. As seen before, increasing one of the parameters leads to deviation from the parabolic profile, which is obtained for $\alpha = 0.0$ and any choice of Λ, because the velocity profile in this case is independet of the relaxation time. The deviation becomes even larger, when the values of the parameters are further increased.

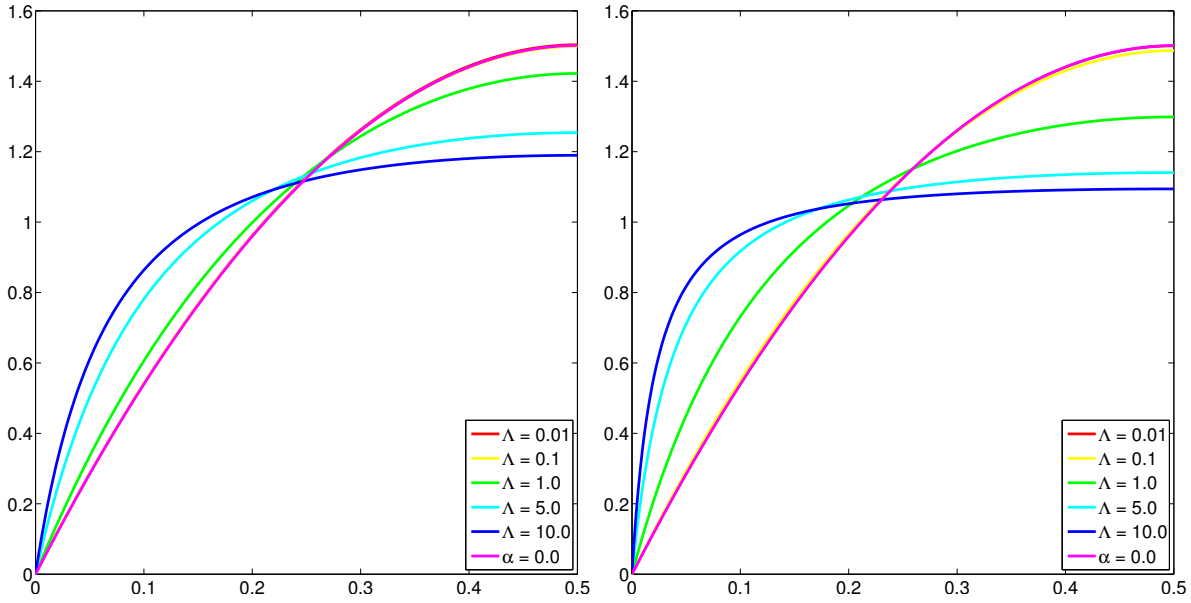

(a) $\alpha = 0.01$ (b) $\alpha = 0.1$

Figure 4: velocity profiles resulting from the Giesekus model for various Λ, α and $\eta_p = 1.0$

2.4. Extension to other models

The previously presented method is applicable to other differential models as well, e.g. the FENE model (c.f. 2.4.1, [9]) or PTT model (c.f. 2.4.2, [10]). The only changes compared to the Giesekus model occur in equation (9), while the equation (7), which results from the Stokes equations, stays the same. Therefore, to transfer the numerical method to any other differential model, it is sufficient to write the corresponding conformation tensor formulation of the chosen viscoelastic model component-by-component, as done in equation (9) for the Giesekus model. Of course, it can not be guaranteed that the resulting nonlinear system can be solved in a decoupled way as before, but applying a coupled solution approach seems promising. But it might as well be possible to solve the nonlinear system analytically, which is the case for the FENE as well as the PTT model (c.f. sections 2.4.1 and 2.4.2, respectively).

In the following sections, the adaption of the method derived in secion 2.2 is performed, so that the fully developed flow profiles for the FENE and PTT model can be determined. Additionally, some examples of resulting profiles are discussed and, by means of the following remarks, the basic procedure of how to transfer the presented method to an arbitrary differential viscoelastic model is outlined.

2.4.1. FENE model

Following [9], the constitutive equation for the conformation tensor $\boldsymbol{\tau}$ introduced by the FENE-CR model reads

$$-\nabla\mathbf{u}\cdot\boldsymbol{\tau}-\boldsymbol{\tau}\cdot\nabla\mathbf{u}^{\top}+\frac{1}{\Lambda}\frac{1}{1-\frac{R^2}{L^2}}\left(\boldsymbol{\tau}-\mathbf{I}\right)=\mathbf{0}, \tag{12}$$

where R^2 is defined as the trace of the conformation tensor, i.e. $R^2=\tau_{11}+\tau_{22}$. When equation (12) is written component-by-component in combination with the momentum part (3a) of the Stokes equations and equation (5) characterizing a fully developed flow, it follows

$$\begin{aligned}
\frac{\partial p}{\partial x} &= \frac{\eta_p}{\Lambda}\frac{\partial\tau_{12}}{\partial y}, && \text{(13a)}\\
-2\tau_{12}\frac{\partial u}{\partial y}+\frac{1}{\Lambda}\frac{1}{1-\frac{R^2}{L^2}}\left(\tau_{11}-1\right) &= 0, && \text{(13b)}\\
-\tau_{22}\frac{\partial u}{\partial y}+\frac{1}{\Lambda}\frac{1}{1-\frac{R^2}{L^2}}\tau_{12} &= 0, && \text{(13c)}\\
\frac{1}{\Lambda}\frac{1}{1-\frac{R^2}{L^2}}\left(\tau_{22}-1\right) &= 0. && \text{(13d)}
\end{aligned}$$

This ODE system will now be used for determining the fully developed flow profiles, i.e. the variables τ_{11}, τ_{12}, τ_{22} and u in case of the FENE model. In other words, the system (13) will be used in algorithm 1 instead of the system (7a) plus (9) resulting from the Giesekus model.

Fortunately, no numerical solution of the nonlinear system is necessary in this case, because the quantities can be calculated analytically for given $\frac{\partial p}{\partial x}$ in the following way. First, τ_{12} is determined by integration of equation (13a) with respect to $\tau_{12}(0.5) = 0$ and additionally, $\tau_{22} = 1$ holds, which can be directly concluded from equation (13d). Next, equation (13c) is solved for $\frac{\partial u}{\partial y}$, which is inserted into equation (13b) and yields τ_{11}. Finally, $\frac{\partial u}{\partial y}$ can be determined from equation (13c) and is integrated to u on the condition $u(0) = 0$. The described procedure results in the expressions listed in equation (14).

$$\tau_{11}^{\text{ana}}(y) = 1 + 2\left(\frac{\partial p}{\partial x}\frac{\Lambda}{\eta_p}(y - 0.5)\right)^2 \tag{14a}$$

$$\tau_{22}^{\text{ana}}(y) = 1 \tag{14b}$$

$$\tau_{12}^{\text{ana}}(y) = \frac{\partial p}{\partial x}\frac{\Lambda}{\eta_p}(y - 0.5) \tag{14c}$$

$$u^{\text{ana}}(y) = \frac{L^2\eta_p}{4\Lambda^2\frac{\partial p}{\partial x}} \ln\left[\frac{1 - \frac{2}{L^2}\left(1 + \left(\frac{\partial p}{\partial x}\frac{\Lambda}{2\eta_p}\right)^2\right)}{1 - \frac{2}{L^2}\left(1 + \left(\frac{\partial p}{\partial x}\frac{\Lambda}{\eta_p}(y - 0.5)\right)^2\right)}\right] \tag{14d}$$

In summary, the numerical method mentioned in algorithm 1 reduces to the numerical calculation of the pressure drop $\frac{\partial p}{\partial x}$. In fact, it is also possible to integrate u^{ana}, whose result correlates to the flow rate (c.f. equation (10)), but unfortunately the resulting expression can not be solved for $\frac{\partial p}{\partial x}$ analytically. Therefore, the introduced numerical method still needs to be applied to determine the fully developed flow profiles for the FENE model, but at least the numerical solution of a nonlinear system of equations is unnecessary.

In figure (5), exemplary results for flow profiles obtained for the FENE model are depicted. Similar to the Giesekus model, the velocity profile shows a shear thinning effect for $\Lambda > 0$, which increases for increasing Λ. The magnitude of the stresses increases as well for increasing Λ and besides, the obtained stress profiles show the same behaviour as those belonging to the Oldroyd-B model. This can already be seen from equations (14a), (14b) and (14c), because the analytical expressions of the stress variables coincide with the terms for the Oldroyd-B model. But the stress profiles must not exactly be the same, because the pressure drop is calculated on the basis of the velocity profile, which is different for the FENE model compared to the Oldroyd-B model.

All in all, the derived method is applicable to the FENE model as well and leads to plausible results, because the obtained profiles show similarities to the Oldroyd-B and

Giesekus model.

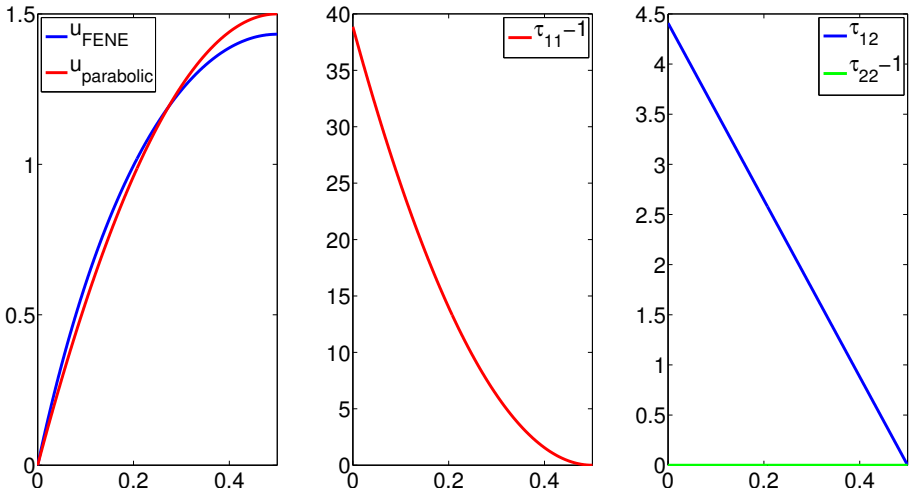

(a) $\Lambda = 1.0$

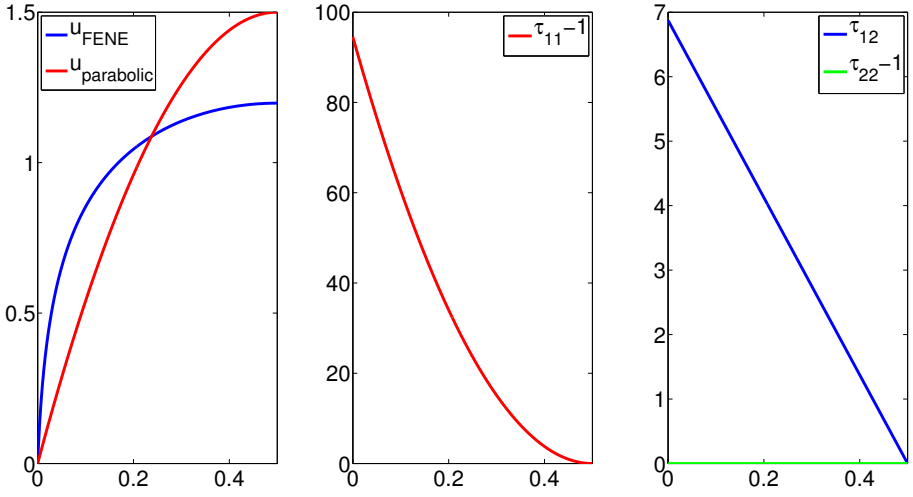

(b) $\Lambda = 5.0$

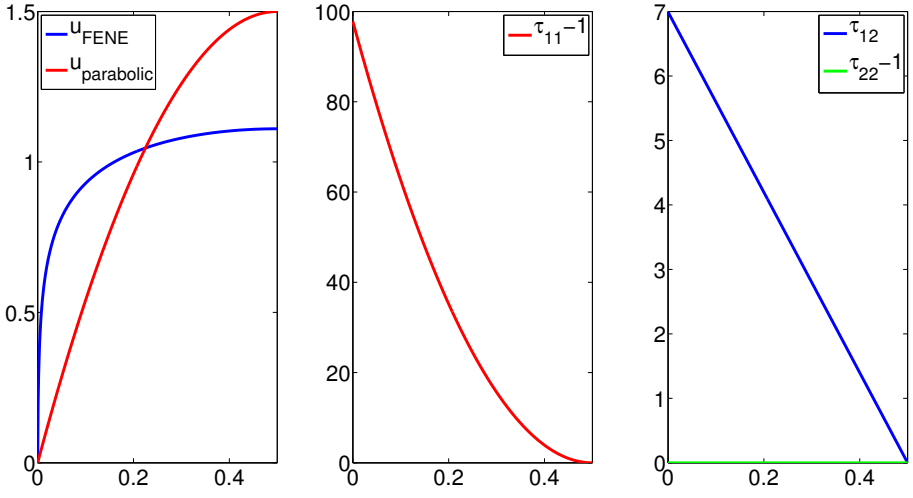

(c) $\Lambda = 10.0$

Figure 5: flow profiles for various Λ, $\eta_p = 1.0$, $L^2 = 100$

2.4.2. PTT model

For the PTT model mentioned in [10] with respect to fully developed flows, the conformation tensor satisfies the constitutive equation

$$-\nabla \mathbf{u} \cdot \boldsymbol{\tau} - \boldsymbol{\tau} \cdot \nabla \mathbf{u}^{\top} + \frac{1}{\Lambda} \exp\left(\varepsilon \operatorname{tr}\left(\boldsymbol{\tau} - \mathbf{I}\right)\right)\left(\boldsymbol{\tau} - \mathbf{I}\right) = \mathbf{0}, \tag{15}$$

which represents the exponential form of the material model with $\varepsilon \in [0, 1]$. Thereby, for $\varepsilon = 0.0$ the Oldroyd-B model is obtained. Similar to the calculations above, in combination with the Stokes equations this constitutive equation results in the nonlinear system

$$\begin{aligned}
\frac{\partial p}{\partial x} &= \frac{\eta_p}{\Lambda} \frac{\partial \tau_{12}}{\partial y}, && \text{(16a)}\\
-2\tau_{12}\frac{\partial u}{\partial y} + \frac{1}{\Lambda}\exp\left[\varepsilon\left(\tau_{11} + \tau_{22} - 2\right)\right]\left(\tau_{11} - 1\right) &= 0, && \text{(16b)}\\
-\tau_{22}\frac{\partial u}{\partial y} + \frac{1}{\Lambda}\exp\left[\varepsilon\left(\tau_{11} + \tau_{22} - 2\right)\right]\tau_{12} &= 0, && \text{(16c)}\\
\frac{1}{\Lambda}\exp\left[\varepsilon\left(\tau_{11} + \tau_{22} - 2\right)\right]\left(\tau_{22} - 1\right) &= 0 && \text{(16d)}
\end{aligned}$$

for the unknowns τ_{11}, τ_{12}, τ_{22} and u. Even for $\varepsilon > 0$, this system of equations can be solved analytically. Again, τ_{12} can be determined by integrating equation (16a) and equation (16d) yields $\tau_{22} = 1$. In an analogous way to the FENE model, equation (16c) is solved for $\frac{\partial u}{\partial y}$, which is then inserted into equation (16b) to determine τ_{11}. At last, $\frac{\partial u}{\partial y}$ is calculated from equation (16c) and integrated to u. The corresponding analytical expressions are

$$\begin{aligned}
\tau_{11}^{\text{ana}}(y) &= 1 + 2\left(\frac{\partial p}{\partial x}\frac{\Lambda}{\eta_p}\left(y - 0.5\right)\right)^2,\\
\tau_{22}^{\text{ana}}(y) &= 1,\\
\tau_{12}^{\text{ana}}(y) &= \frac{\partial p}{\partial x}\frac{\Lambda}{\eta_p}\left(y - 0.5\right),\\
u^{\text{ana}}(y) &= \frac{\eta_p}{4\varepsilon\Lambda^2\frac{\partial p}{\partial x}}\left(\exp\left[2\varepsilon\left(\frac{\partial p}{\partial x}\frac{\Lambda}{\eta_p}\left(y - 0.5\right)\right)^2\right] - \exp\left[\frac{\varepsilon}{2}\left(\frac{\partial p}{\partial x}\frac{\Lambda}{\eta_p}\right)^2\right]\right).
\end{aligned}$$

In contrast to the FENE model, the flow rate can not be determined analytically, because the integral of u is not solvable exactly. So again, the numerical method needs to be applied to calculate the correct pressure drop $\frac{\partial p}{\partial x}$ for a certain flow rate.

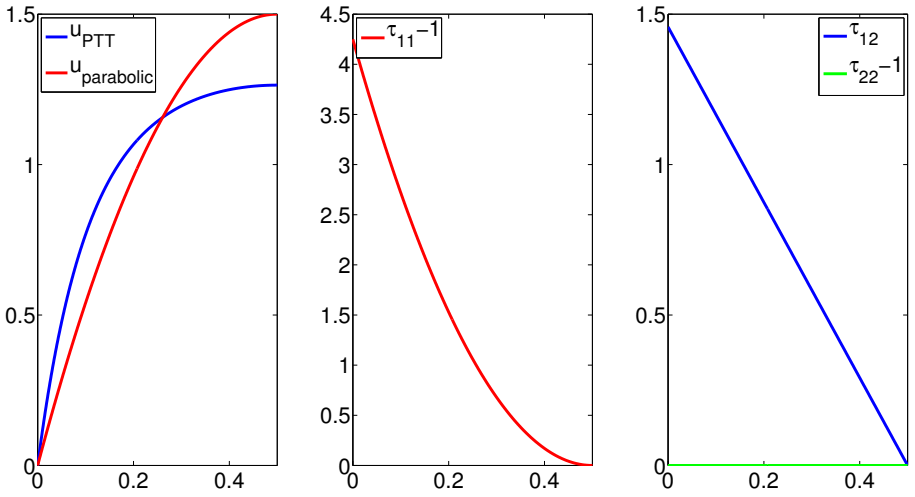

(a) $\Lambda = 1.0$

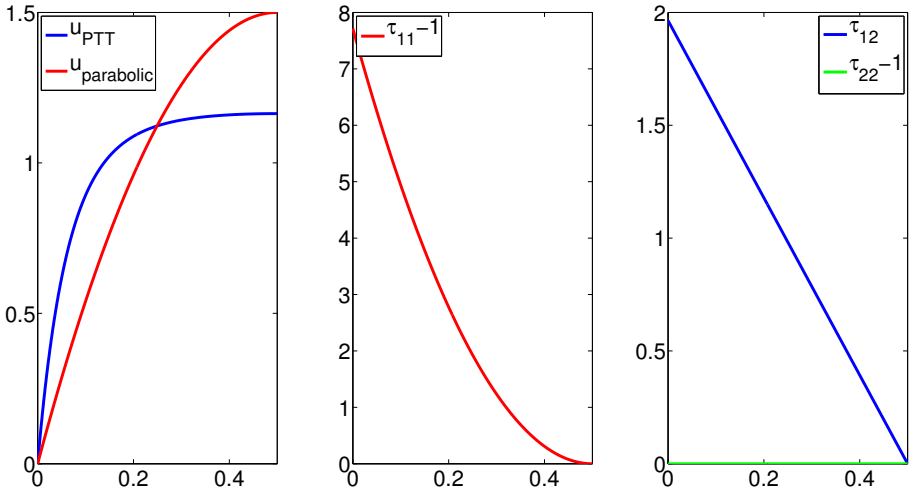

(b) $\Lambda = 5.0$

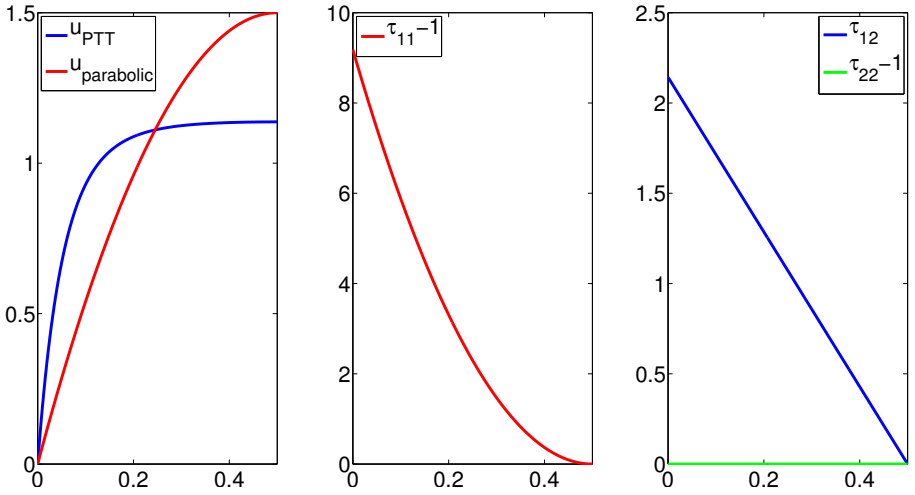

(c) $\Lambda = 10.0$

Figure 6: flow profiles for various Λ, $\varepsilon = 0.5$, $\eta_p = 1.0$

Several examples of flow profiles resulting from the PTT model are shown in figure 6.

As before, the obtained velocity profile shows a shear thinning behaviour and the stress profiles are related to the corresponding profiles for the FENE or Oldroyd-B model, i.e. τ_{11} shows a quadratic behaviour, τ_{12} is linear and τ_{22} constant.

In a nutshell, similar to the results for the FENE model, the flow profiles determined for the PTT model obey a reasonable behaviour.

If instead of the exponential form, the linear form

$$-\nabla\mathbf{u}\cdot\boldsymbol{\tau}-\boldsymbol{\tau}\cdot\nabla\mathbf{u}^{\top}+\frac{1}{\Lambda}\left(1+\varepsilon\,\mathrm{tr}\left(\boldsymbol{\tau}-\mathbf{I}\right)\right)\left(\boldsymbol{\tau}-\mathbf{I}\right)=\mathbf{0}$$

of the PTT model is used (c.f. [10]), the same analytical stress functions can be derived, but the velocity function u differs and takes a polynomial form. Unfortunately, according to the exponential form, the correct pressure drop can not be determined analytically and the application of the numerical method is necessary.

Of course, the method to determine numerically fully developed flow profiles for differential viscoelastic models is also applicable to more complex material models, where the resulting nonlinear system with respect to τ_{11}, τ_{12}, τ_{22} and u can not be solved analytically. In this case, the decoupled solution approach can be discarded and it might be useful to solve the system in a coupled way. The corresponding solution process is explained in more detail in the next section, where this so-called monolithic solution approach is applied as well.

3. Determine flow profiles for fluids with solvent part

Up to now, we only focused on the case $\eta_s = 0$, i.e. the considered fluids do not contain any solvent material. As will be shown in this section, the numerical method introduced in section 2.2 can be more or less easily extended to fluids which possess a solvent part.

3.1. The nonlinear ODE system

Once viscoelastic fluids containing solvent material are modeled with the Stokes equations, the extra stress tensor $\mathbf{T}$ in equation (1) depends not only on the elastic part described by the conformation tensor $\boldsymbol{\tau}$ (c.f. equation (2)), but also on a viscous stress component including the rate of deformation tensor $\mathbf{D}=\frac{1}{2}\left(\nabla\mathbf{u}+\nabla\mathbf{u}^{\top}\right)$. Thus, following [3], the formulation of the extra stress tensor reads

$$\mathbf{T}=2\eta_s\mathbf{D}+\frac{\eta_p}{\Lambda}\left(\boldsymbol{\tau}-\mathbf{I}\right), \tag{17}$$

where the solvent and polymer viscosities, η_s and η_p, respectively, are related to each other in combination with the total viscosity η_0 by

$$\eta_0 = \eta_s + \eta_p, \quad \eta_s = \beta\eta_0, \quad \beta \in [0,1].$$

Obviously, the case of pure polymer melts is obtained for $\beta = 0.0$.

When the derivation of the nonlinear ODE system for the Giesekus model in section 2.2 is repeated, but for equations (1) and (4) in combination with equation (17) instead of (2), one ends up with the ODE system

$$\begin{aligned}
\frac{\partial p}{\partial x} &= \eta_s \frac{\partial^2 u}{\partial y^2} + \frac{\eta_p}{\Lambda}\frac{\partial \tau_{12}}{\partial y} && \text{(18a)}\\
\frac{\partial p}{\partial y} &= \frac{\eta_p}{\Lambda}\frac{\partial \tau_{22}}{\partial y} && \text{(18b)}\\
-2\tau_{12}\frac{\partial u}{\partial y} + \frac{1}{\Lambda}\left[\tau_{11} - 1 + \alpha\left(\left(\tau_{11}-1\right)^2 + \tau_{12}^2\right)\right] &= 0 && \text{(18c)}\\
-\tau_{22}\frac{\partial u}{\partial y} + \frac{1}{\Lambda}\left[\tau_{12} + \alpha\left(\left(\tau_{11}-1\right)\tau_{12} + \tau_{12}\left(\tau_{22}-1\right)\right)\right] &= 0 && \text{(18d)}\\
\frac{1}{\Lambda}\left[\tau_{22} - 1 + \alpha\left(\tau_{12}^2 + \left(\tau_{22}-1\right)^2\right)\right] &= 0. && \text{(18e)}
\end{aligned}$$

Note, that the constitutive equation itself, i.e. equation (4) for the Giesekus model, stays unchanged, because the solvent part of the fluid is considered in the momentum equation of the Stokes equations (1), only.

3.2. The numerical method

Basically, algorithm 1 can also be used for solving the nonlinear system (18), but some few changes are necessary. Unfortunately, the change in equation (18a) compared to equation (3a) implies, that the basic assumption $\frac{\partial p}{\partial x} = \text{const}$ for the case $\beta = 0.0$ does not hold any more for $\beta > 0$, because an additional term appears in equation (18a). That is why it is not possible to compute τ_{11} explicitly if $\frac{\partial p}{\partial x}$ is known and therefore a decoupled solution method is not applicable anymore.

Thus, it might be helpful choosing a coupled solution approach, i.e. we replace steps 6, 7 and 8 of algorithm 1 with an application of a monolithic nonlinear solver, e.g. Newton's method, for u, τ_{11}, τ_{12} and τ_{22}. Thereby, the appearing derivatives can be approximated by Finite Difference schemes, which implies direct solutions for u instead of $\frac{\partial u}{\partial y}$, i.e. no separate integration of $\frac{\partial u}{\partial y}$ is necessary.

3.3. Numerical results

Some results obtained with the method described in section 3.2 are presented in figure 7. Already for a quite small relaxation time of $\Lambda = 2.5$ (c.f. figure 7(a)), large deviations of the profiles for $\beta > 0.0$ to those for $\beta = 0.0$ can be observed. The velocity profiles

for $\beta \to 1.0$ reform incrementally to a parabolic shape, which correlates to the velocity profile of a Newtonian fluid, i.e. $\beta = 1.0$. Just as the velocity profiles, the stress profiles for $\beta > 0$ deviate significantly from the profiles for pure melts. Furthermore, the course of the "solvent" stress profiles does not even qualitatively matches that for pure melts, which in contrast holds for the velocity profiles. The described behaviour of the flow profiles is recurred for larger relaxation times, e.g. for $\Lambda = 10.0$ in figure 7(b), in an intensified manner, especially regarding the stress variables. For increasing β, the profiles seem to converge towards a singularity in the middle of the channel, i.e. at the position $y = 0.5$. However, this singularity has no big impact on the numerical results in actual two-dimensional simulations, because for $\beta \to 1$ the amount of the stress included in the momentum equation tends to 0.

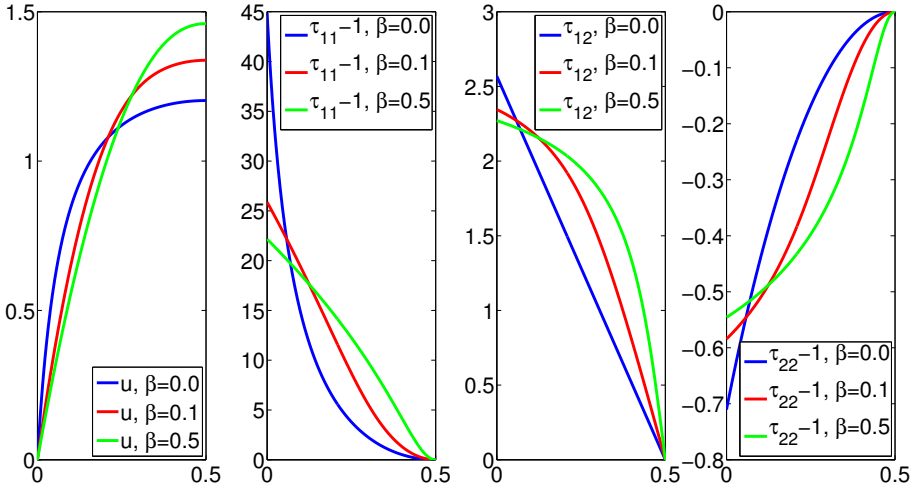

(a) $\Lambda = 2.5$

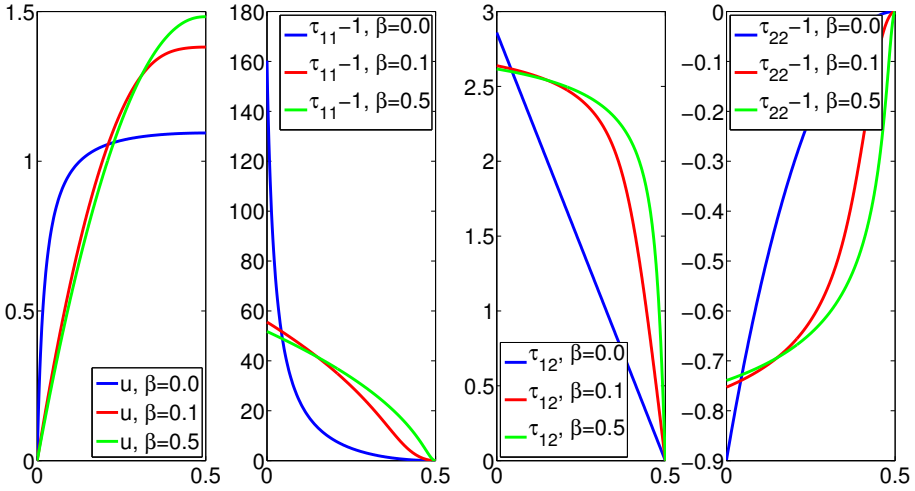

(b) $\Lambda = 10.0$

Figure 7: flow profiles for various Λ and β, where $\alpha = 0.1$ and $\eta_0 = 1.0$

4. Validation of the results for the Giesekus model

To substantiate, that the flow profiles computed with algorithm 1 are correct and suitable for actual flow simulations, we perform a Finite Element simulation of a Poiseuille flow through a plane channel. The computational domain used in the following, is a rectangular channel in the (x, y) plane, pictured in figure 8, which can be described by $(x, y) \in [0, 5] \times [0, 1]$.

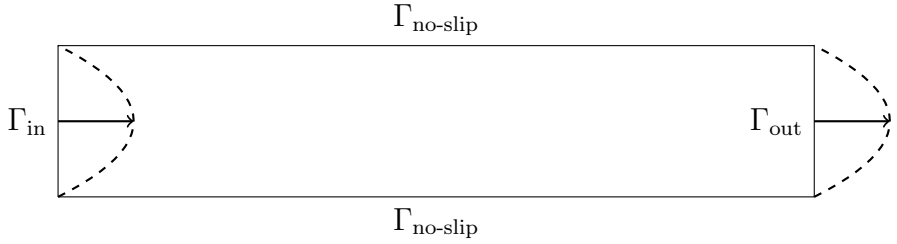

Figure 8: computational domain for flow through plane channel

In the simulations, we consider a viscoelastic fluid modeled with the Giesekus model. Additionally, we set Dirichlet boundary conditions at every boundary segment of the computational domain, which means that fully developed flow profiles are applied as in- and outflow boundary conditions at Γ_{in} and Γ_{out} for the velocity as well as the stress variables. Naturally, we choose the flow profiles determined with algorithm 1 as in- and outflow profiles. The upper and lower boundaries are set to "no-slip" boundaries, i.e. we prescribe $\mathbf{u} = \mathbf{0}$ on $\Gamma_{\text{no-slip}}$. For the stresses, a constant value, resulting from the computed profiles, is prescribed on $\Gamma_{\text{no-slip}}$. That means, we prescribe only Dirichlet boundaries in the computational domain and renounce Neumann boundaries.

We can accept the flow profiles obtained with algorithm 1 to be the fully developed flow profiles for a certain differential viscoelastic model, if the contour lines of the channel flow obey a purely straight behaviour. This straight behaviour is desired, because straight contour lines would imply, that the same profile of the associated variable is obtained on every cutline of the channel in y-direction, including the prescribed in- and outflow edge. This means, that there is no change in the flow, which yields in turn, that the applied in- and outflow profiles are the "analytical" profiles belonging to the chosen model.

First, in section 4.1, focus is placed on the detailed validation of the flow profiles of the Giesekus model resulting for pure polymer melts, i.e. $\beta = 0.0$. Therefore, we will consider simulations with a moderate relaxation time in section 4.1.1 as well as higher relaxation times in section 4.1.2. Finally, we will shortly focus on the simulation of flows, where the fluid described by the Giesekus model contains solvent part (c.f. 4.2).

4.1. Simulation of pure polymer melts

4.1.1. Simulations with moderate relaxation time

First, we want to show, that the flow profiles are suitable for moderately high relaxation times. Therefore, we use a coarse mesh (level 0) to discretize the spacial domain, consisting of five quadratic elements. Further details of the computational mesh can be found in table 1.

level	elements	nodes	edges	degrees of freedom
0	5	12	16	180
1	20	33	52	585
2	80	105	184	2085
3	320	369	688	7845
4	1280	1377	2656	30405
5	5120	5313	10432	119685

Table 1: mesh information

The material and model parameters in the following simulations are set to $\Lambda = 1.0$, $\eta_p = 1.0$ and $\alpha = 0.1$, for which algorithm 1 leads to the flow profiles shown in figure 9.

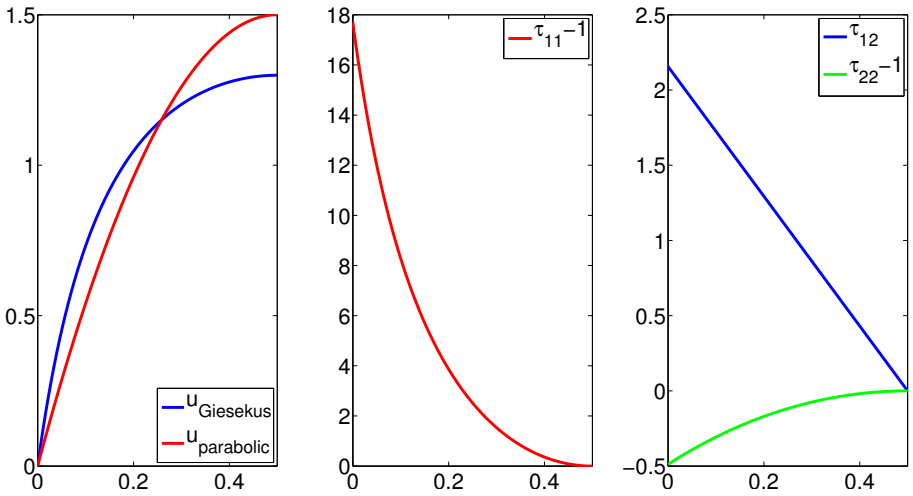

Figure 9: Velocity and stress profiles for $\Lambda = 1.0$, $\eta_p = 1.0$, $\alpha = 0.1$

To run the simulations, the same numerical method and software as in [3] is used, i.e. especially techniques such as "log-conformation reformulation" (LCR) and "Edge-Oriented FEM" stabilization (EO-FEM) are applied. Some results obtained for these simulations can be found in figures 10 to 13, where the x-component u of the velocity and the components ψ_{11}, ψ_{12} and ψ_{22} of the LCR variable $\boldsymbol{\psi}$ are pictured. The results are obtained on mesh level 4, i.e. on the mesh resulting from the coarse mesh after four refinements, and with EO-FEM stabilization with parameter $\gamma = 0.1$.

The depicted flows already show nearly straight contour lines, that is why we can state, that the flow profiles determined with algorithm 1, used as Dirichlet in- and outflow boundary conditions, lead to a nearly smooth flow. Furthermore, on the basis of the mentioned profiles, we see, that also in the middle of the channel, i.e. at $x = 2.5$, the flow profiles match the prescribed in- and outflow profiles.

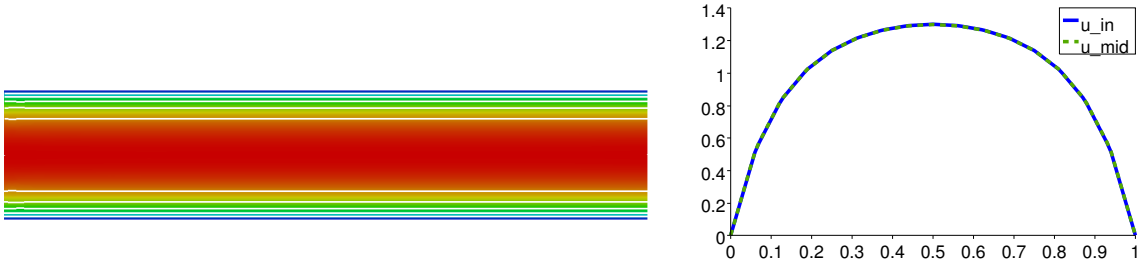

(a) contour lines (b) profiles at $x = 0$ and $x = 2.5$

Figure 10: resulting velocity for $\Lambda = 1.0$, $\alpha = 0.1$ on level 4 with $\gamma = 0.1$

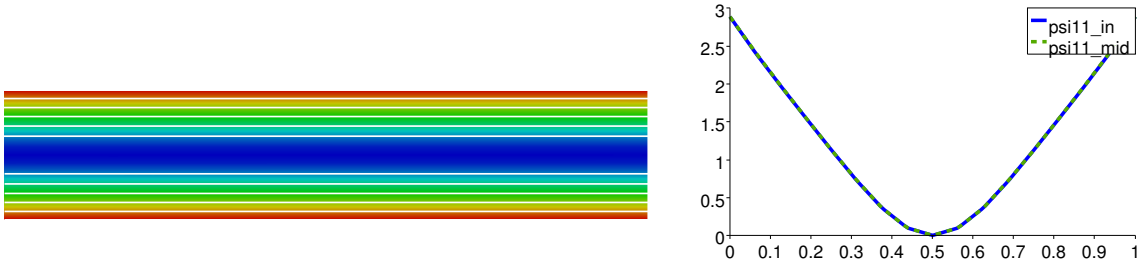

(a) contour lines (b) profiles at $x = 0$ and $x = 2.5$

Figure 11: resulting ψ_{11} for $\Lambda = 1.0$, $\alpha = 0.1$ on level 4 with $\gamma = 0.1$

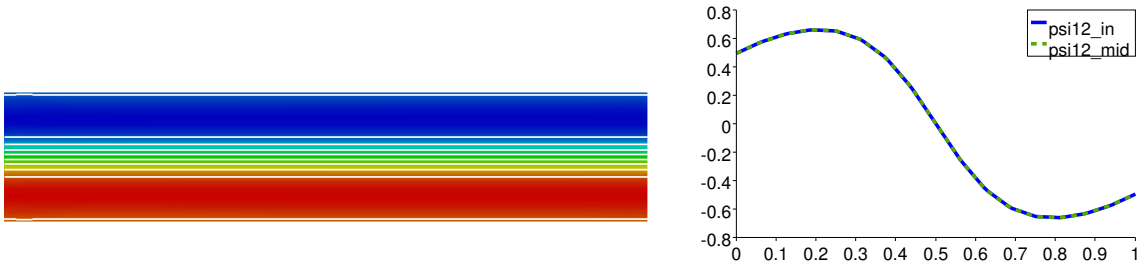

(a) contour lines (b) profiles at $x = 0$ and $x = 2.5$

Figure 12: resulting ψ_{12} for $\Lambda = 1.0$, $\alpha = 0.1$ on level 4 with $\gamma = 0.1$

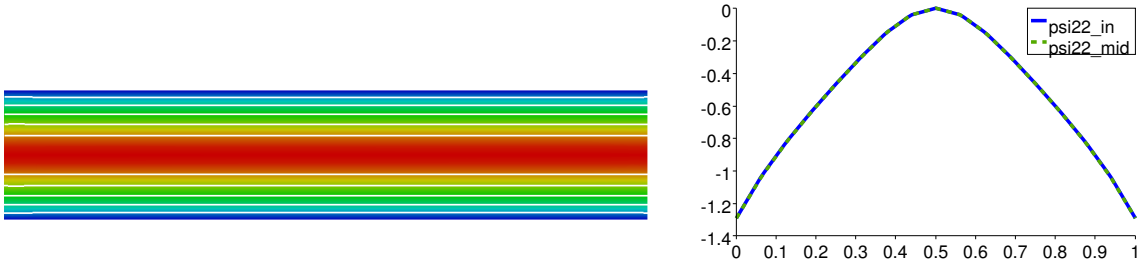

(a) contour lines (b) profiles at $x = 0$ and $x = 2.5$

Figure 13: resulting ψ_{22} for $\Lambda = 1.0$, $\alpha = 0.1$ on level 4 with $\gamma = 0.1$

Collectively, it is substantiated, that the flow profiles determined with algorithm 1, coincide with the flow profiles resulting from two-dimensional simulations of a Poiseuille flow of a viscoelastic fluid desribed with the Giesekus model. This implies, that the numerically determined flow profiles actually are the fully developed flow profiles belonging to the Giesekus model.

4.1.2. Simulations with high relaxation time

In section (4.1.1) we pointed out, that algorithm 1 yields the fully developed flow profiles of a viscoelastic fluid with respect to the Giesekus model, at least for moderately high relaxation times. In this section, we want to investigate the behaviour of a Poiseuille flow through a plane channel, when the relaxation time is chosen larger. Therefore, the material and model parameters in the following simulations are set to $\Lambda = 5.0$, $\eta_p = 1.0$ and $\alpha = 0.1$, which results in the flow profiles depicted in figure 14.

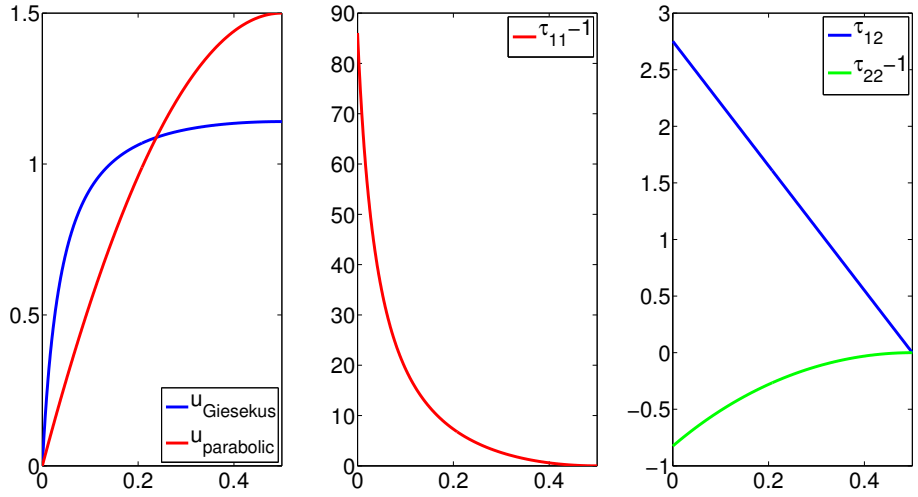

Figure 14: Velocity and stress profiles for $\Lambda = 5.0$, $\eta_p = 1.0$, $\alpha = 0.1$

The rest of the setting, i.e. boundary conditions and coarse mesh, corresponds to the configuration used in the previous section. But the choice of the "naive" coarse mesh, referred to in table 1, could lead to numerical oscillations. That is, because compared

to the flow profiles for $\Lambda = 1.0$, c.f. figure 9, the flow profiles for $\Lambda = 5.0$ show a much steeper rise near the wall of the channel and the resulting large gradients might not be resolved in a sufficient manner by the naive mesh.

Nevertheless, a smooth flow, showing nearly straight contour lines, can be obtained by choosing a sufficiently high refinement level of the mesh 1 and a suitable EO-FEM stabilization parameter γ. Exemplary numerical results on the example of the component ψ_{12} of the LCR variable $\boldsymbol{\psi}$ are depicted in figure 15. We focus on this component only, because the other variables show a similar behaviour.

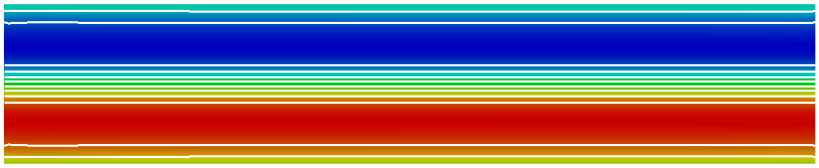

Figure 15: contour lines of ψ_{12} for $\Lambda = 5.0$, $\alpha = 0.1$ on L5 of naive mesh with $\gamma = 0.1$

In figure 16, the resulting flow on mesh level 4 is shown. It becomes clear, that it is necessary to choose either a higher level of the naive mesh, or a larger stabilitzation parameter to get a smooth flow. Summing up, on level 5 the numerical solution looks satisfactory, but on level 4 we get a disturbed solution.

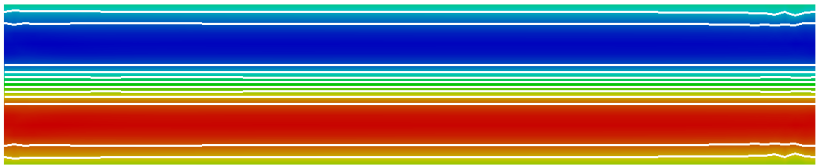

Figure 16: contour lines of ψ_{12} for $\Lambda = 5.0$, $\alpha = 0.1$ on L4 of naive mesh with $\gamma = 0.1$

Of course, one can not expect to resolve sufficiently the large gradients near the wall of the channel on a low level of the naive mesh. Thus, a high numerical effort is necessary to get acceptable results. To reduce the amount of numerical costs, we will use an adapted mesh in the following simulations of a Poiseuille flow in a plane channel, to resolve the large gradients near the channel wall in an improved way without dramatically increasing the mesh refinement.

The used adapted mesh and the corresponding details are summarized in figure 17 and table 2, respectively.

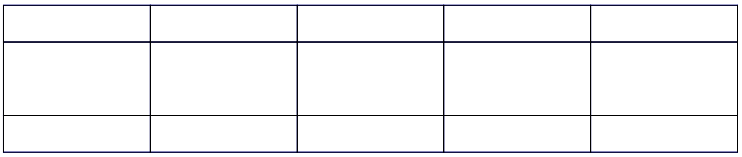

Figure 17: adapted mesh

level	elements	nodes	edges	degrees of freedom
0	15	24	38	430
1	60	77	136	1545
2	240	273	512	5845
3	960	1025	1984	22725
4	3840	3969	7808	89605

Table 2: details on the adapted mesh 17

The results depicted in figure 18 show, that a numerical solution on level 3 of mesh 17 with relatively small γ already leads to a quite smooth flow, based on the contour lines of ψ_{11} (c.f. figure 18(a)). Also the profiles in figure 18(b) do not exhibit visible deviations between the inflow profile and the profile in the middle of the channel.

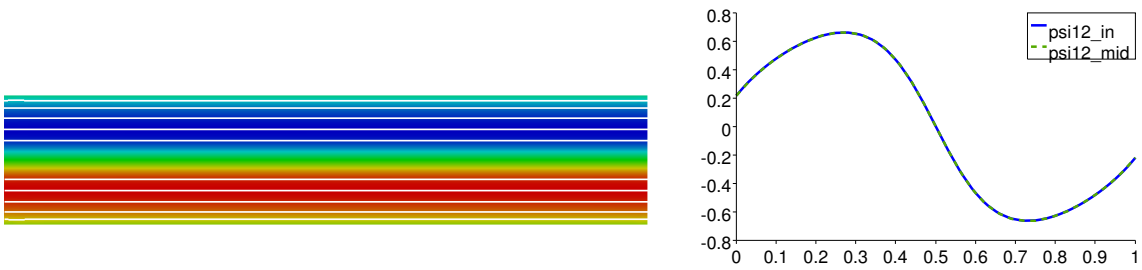

(a) contour lines

(b) profiles at $x = 0$ and $x = 2.5$

Figure 18: resulting ψ_{12} for $\Lambda = 5.0$, $\alpha = 0.1$ on L3 of mesh 17 with $\gamma = 0.01$

These results are obtained with 22725 degrees of freedom and $\gamma = 0.01$, while the corresponding results in figure 15 are of the same quality, although a number of degrees of freedom, which is six times higher, was used, namely 119685 (c.f. table 2). Thus, we can conclude, that satisfying numerical results are obtained on a low level of the adapted mesh, which have a similar quality as those results generated on a high level of the naive mesh.

All in all we can state, that the flow profiles, obtained with algorithm 1, applied as Dirichlet in- and outflow conditions to a Poiseuille flow in a plane channel, result in a smooth flow, even for relatively high relaxation times. This means, that these profiles are

equivalent to the fully developed flow profiles of a viscoelastic fluid, without solvent part, modeled with the Giesekus model.

4.2. Simulation of fluids containing solvent material

Similar to previous sections, we will now focus on simulating a flow of a viscoelastic fluid, which contains solvent material as well, through a plane channel. Again, besides the numerical techniques applied in [3], we use the same computational domain and mesh mentioned in section 4.1.1. Furthermore, we choose $\Lambda = 10.0$, $\alpha = 0.1$, $\eta_0 = 1.0$ plus $\beta \in \{0.1, 0.5\}$ and prescribe the fully developed flow profiles depicted in figure 7(b) as in- and outflow data. As before, we will discuss the results of the Finite Element simulations on the example of the ψ_{12} component of the LCR variable $\boldsymbol{\psi}$.

The resulting flow for $\beta = 0.1$ is presented in figure 19. Obviously, a very smooth flow is obtained, which can be concluded from the contour lines as well as from the flow profiles.

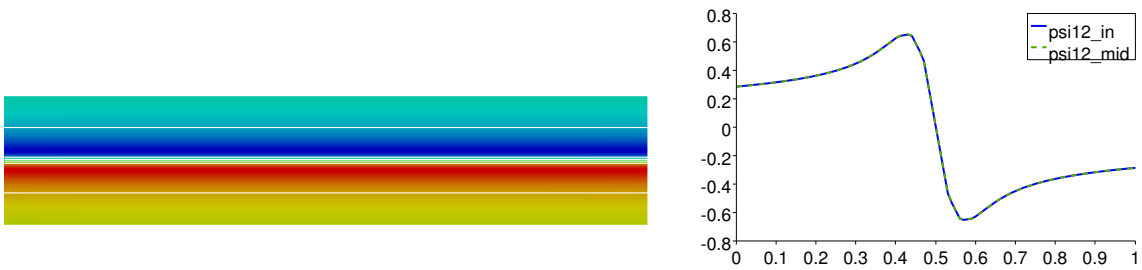

(a) contour lines (b) profiles at $x = 0$ and $x = 2.5$

Figure 19: resulting ψ_{12} for $\Lambda = 10.0$, $\alpha = 0.1$, $\eta_0 = 1.0$ and $\beta = 0.1$ on L5 with $\gamma = 0.1$

When the amount of solvent material is increased, e.g. choosing $\beta = 0.5$, the contour lines still look very smooth (c.f. figure 20(a)), but the profile at $x = 2.5$, i.e. in the middle of the channel in x-direction, shows slight deviations from the inflow data (c.f. figure 20(b)). This behaviour can also be observed for all other stress components, which probably occurs because of the large stress gradients near $y = 0.5$, i.e. at the centerline of the channel in y-direction, and could be resolved by increasing the mesh level.

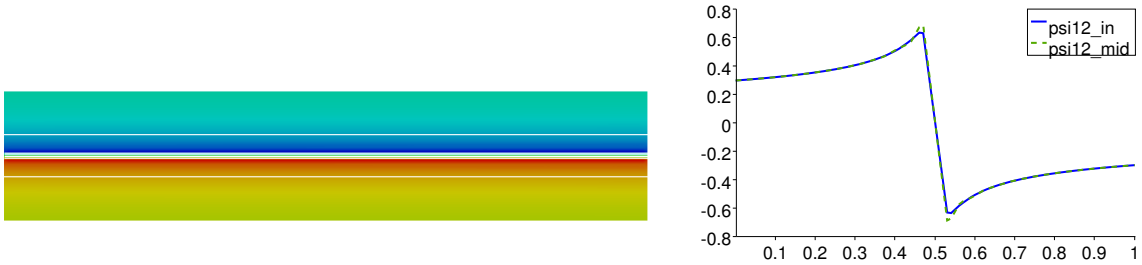

(a) contour lines (b) profiles at $x = 0$ and $x = 2.5$

Figure 20: resulting ψ_{12} for $\Lambda = 10.0$, $\alpha = 0.1$, $\eta_0 = 1.0$ and $\beta = 0.5$ on L5 with $\gamma = 0.1$

But nevertheless, the in- and outflow profiles show a high accordance to the profiles gained in the two-dimensional simulations, which is why the profiles calculated with algorithm 1 for $\beta > 0$ can be regarded as fully developed flow profiles. Admittedly, it is still an open question why the stress profiles take such a strange form for $\beta \to 1$. On the one hand one would expect the behaviour $\boldsymbol{\tau} \to \mathbf{I}$ for $\beta \to 1$, because the elastic stress should vanish if the considered fluid contains almost only Newtonian material. But $\boldsymbol{\tau} = \mathbf{I}$ is no solution of the nonlinear system (18), even for $\beta = 1.0$. Fortunately this is not inconsistent with the extra stress tensor, because on the other hand, $\eta_p \to 0$ for $\beta \to 1$ holds, which implies that the elastic stress vanishes and therefore no contribution is added to the extra stress. So the actual form of the elastic stress components in the limit $\beta \to 1$ is not that important.

Again, also for viscoelastic fluids containing solvent part, the numerically calculated flow profiles coincide with the profiles determined in two-dimensional simulations, which validates the numerical method also with respect to considering a solvent part in the simulated fluids.

5. Conclusion and outlook

In summary, we could state, that the fully developed flow profiles for the Giesekus model generated with the described method show a physically correct behaviour. Also in comparison to the Oldroyd-B model, these profiles show feasible properties. The generated flow profiles can be used as prescribed inflow profiles if Dirichlet boundary conditions are applied, which would guarantee a fully developed inflow in numerical simulations.

In this paper, we also performe two-dimensional Finite Element simulations to show, that the presented numerical method leads to suitable flow profiles for simulations of polymer melts, i.e. viscoelastic fluids without any solvent part, modeled with the Giesekus model. Therefore, we prescribe the obtained flow profiles as Dirichelt in- and outflow conditions of a flow through a plane channel, which leads to a smooth, straight flow inside the whole domain. This confirms, that the flow profiles match the Giesekus model.

Additionally, we validated the approach for determining the flow profiles for viscoelastic fluids containing solvent part. Besides the Giesekus model, the method is extended to also consider other differential models such as PTT and FENE, which leads to satisfactory results as well.

Naturally, the numerical applications, covered in this paper, only touch the full set of configurations, where it might be necessary to consider fully developed flow profiles. For example, in this work we simply focused on two-dimensional simulations. The question may arise, how to apply the presented method to three-dimensional simulations. If rotation-symmetric geometries are concerned, the system of equations to determine the flow variables needs to be transformed into a system depending on cylindrical coordinates.

In contrast, in the cartesian coordinate system, the corresponding system of equations possesses additional equations and unknowns due to the additional spacial dimension. Another expansion of the method is necessary, when the modeling approach changes. As mentioned in [8], the quality of differential models for viscoelastic fluids can be improved, when multiple relaxation times or multiple stress tensors, respectively, are introduced. This would lead to an increasing number of equations, which need to be considered to determine the flow profiles, because each stress tensor requires its own tensorial equation.

Another useful application of fully developed flow profiles is to apply them as outflow profiles in numerical simulations. Following [7], the use of Neumann boundary conditions at the outflow of many geometries leads to numerically disturbed results, which occurs in the previously described framework for pure polymer melts, too - even for simple geometries. When Neumann boundary conditions are applied instead of Dirichlet boundary conditions at Γ_{out}, in most cases we were not able to generate numerical solutions at all for the considered configuration. But once results could be obtained, e.g. the disturbed flow depicted in figure 21, these results can be classified as "wrong", because there are no physical effects in the channel which should influence the flow in any way, but to stay unchanged.

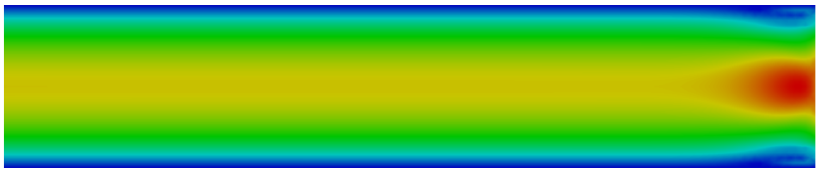

(a) u-velocity flow field

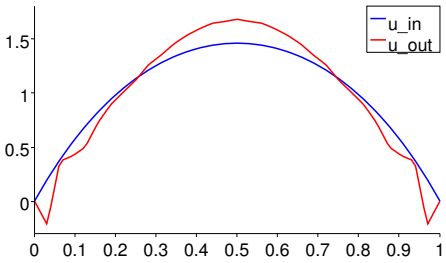

(b) inflow and outflow u-profile

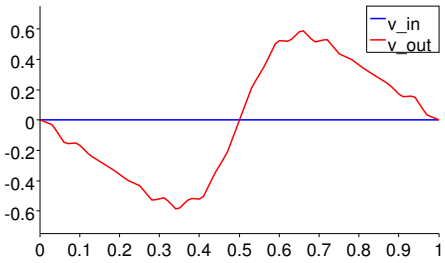

(c) inflow and outflow v-profile

Figure 21: simulated flow for Neumann outflow with $\Lambda = 0.2$, $\alpha = 0.1$ and $\gamma = 0.1$

Hence we suppose, that large numerical oscillations occur, which can not be handled with the numerical method, even when stabilization is applied.

When flow simulations on a more complex computational domain are considered, e.g. the simulations performed in [3], the flow will change due to the geometry. Therefore, the exact outflow profile might be unknown, because the flow still could be disturbed at

the outflow edge of the domain. To avoid oscillations, which occur by applying Neumann outflow conditions, one could elongate the considered computational domain by adding an "outflow channel" to the actual domain. At the end of this channel, the fully developed profiles could be prescribed as Dirichlet outflow conditions. By doing so, the flow in the actual domain is at most influenced slightly, and at the same time no numerical oscillations occur at the outflow edges.

Thus, the presented numerical method to determine fully developed flow profiles for viscoelastic fluids described with differential models is just a starting point to develop improved techniques which can be applied to more complex configurations. But nevertheless, the obtained flow profiles are equivalent to the fully developed profiles, which ensures, that these profiles are suitable for many numerical simulations of viscoelastic fluids.

References

[1] Bonito, A., and Burman, E.: *A continuous interior penalty method for viscoelastic flows*, SIAM Journal on Scientific Computing, 30, 3, 1156, 2008

[2] Choi, H. Ch., and Yoo, J. Y.: *On the steady simple shear flows of the one-mode Giesekus fluid*, Rheo]ogica Acta, 28, 1, 13, 1989

[3] Damanik, H., Hron, J., Ouazzi, A., and Turek, S.: *A monolithic FEM approach for the log-conformation reformulation (LCR) of viscoelastic flow problem*, Journal of Non-Newtonian Fluid Mechanics, 165, 1105, 2010

[4] Fattal, R., and Kupferman, R.: *Time-dependent simulation of viscoelastic flows at high Weissenberg number using the log-conformation representation*, Journal of Non-Newtonian Fluid Mechanics, 126, 23, 2005

[5] Graebling, D., and Joie, J.: *Numerical simulation of polymer flows using non-conforming finite elements*, Computers and Fluids, 79, 178, 2013

[6] Guillopé, C. and Saut, J. C.: *Existence results for the flow of viscoelastic fluids with a differential constitutive law*, Nonlinear Analysis, Theory, Methods and Applications, 15, 9, 849, 1990

[7] Heywood, J. G., Rannacher, R., and Turek, S.: *Artificial boundaries and flux and pressure conditions for the incompressible Navier-Stokes equations*, International Journal for Numerical Methods in Fluids, 22, 325, 1992

[8] Larson, R.: *Constitutive equations for polymer melts and solutions*, Butterworths, 1988, ISBN: 0-409-90119-9

[9] Paulo, G.S., et al.: *Numerical solution of the FENE-CR model in complex flows*, Journal of Non-Newtonian Fluid Mechanics, 204, 50, 2014

[10] Phan Thien, N.: *A nonlinear network viscoelastic model*, Journal of Rheology, 22, 259, 1978